

Sensor Development for the CMS Pixel Detector

T. Rohe[†], D. Bortoletto^{*}, V. Chiochia[‡], L. M. Cremaldi^{**}, S. Cucciarelli^{||}, A. Dorokhov^{†‡},
M. Konecki^{||}, K. Prokofiev^{†‡}, C. Regenfus[‡], D. A. Sanders^{**}, S. Son^{*}, T. Speer[‡], M. Swartz[§]

[†]Paul Scherrer Institut, Villigen, Switzerland ^{*}Purdue University, Task G, West Lafayette, IN 47907, USA

[‡]Physik Institut der Universität Zürich, Switzerland

^{**}University of Mississippi, Department of Physics and Astronomy, University, MS 38677, USA

^{||}Institut für Physik der Universität Basel, Switzerland [§]Johns Hopkins University, Baltimore, Md., USA

Abstract—This paper reports on a current R&D activity for the sensor part of the CMS pixel detector. Devices featuring several design and technology options have been irradiated up to a proton fluence¹ of $1 \times 10^{15} \text{ n}_{\text{eq}}/\text{cm}^2$ at the CERN PS. Afterwards they have been bump bonded to unirradiated readout chips. The chip allows a non zero suppressed full analogue readout and therefore a good characterization of the sensors in terms of noise and charge collection properties. The samples have been tested using high energy pions in the H2 beam line of the CERN SPS in June and September 2003. The results of this test beam are presented and the differences between the sensor options are discussed.

I. INTRODUCTION

The CMS experiment, currently under construction at the Large Hadron Collider (LHC) at CERN (Geneva, Switzerland), will contain a hybrid pixel detector for tracking and vertexing. It will consist in its final configuration of three barrel layers and two end disks at each side. The barrels will be 53 cm long and placed at radii of 4.3 cm and 7.2 cm while the third layer at 11.0 cm will be added later to provide a 3 layer system at high luminosity. The end disks are located at a mean distance to the interaction point of 32.5 cm and 46.5 cm. The whole system will provide three high resolution space points up to a pseudorapidity² of $|\eta| < 2.2$. A total area of about 0.8 m^2 in the barrels will be covered by about 800 modules and 0.28 m^2 by 96 modules, shaped like turbine blades, in the disks.

In order to achieve the best vertex position measurement the spatial resolution of the sensor should be as good in the z -direction (parallel to the beam line) as in (r, ϕ) and therefore almost a squared pixel shape with a pitch of $100 \times 150 \mu\text{m}^2$ was adopted. To improve the spatial resolution analog interpolation between neighboring channels will be performed. The strong Lorentz deflection in the (r, ϕ) -direction caused by CMS' 4 T magnetic field is used to distribute the signal over several channels. Hence the detectors are not tilted in the barrel layers. The resolution along the z -axis is determined by the pixel pitch in the region with low pseudorapidity and by charge sharing if the tracks hit the sensors under an angle where the typical cluster size can exceed values of 6 or 7. The best resolution will be reached at the point where the charge is distributed over about two pixels. In the disks where the charge carrier

drift is hardly affected by the magnetic field the modules are tilted about 20° resulting in a turbine like geometry.

This paper reports on the development of the sensor part of the system. A general overview on the CMS pixel project is given in ref. [1]. Because of the harsh radiation environment at the LHC the technical realization of the pixel detector is extremely challenging. All components of the pixel detector are specified to remain operational up to a particle fluence of at least $6 \times 10^{14} \text{ n}_{\text{eq}}/\text{cm}^2$.

This implies that the pixel sensors have to deliver a sufficiently high signal until the end of their life time. The final readout chips feature built-in data sparcification with a threshold set to 2000-3000 electrons in order to suppress noise hits. With a sensor thickness of $285 \mu\text{m}$, a minimum ionizing particle creates about 22 000 electron-hole pairs (most probable value). However, with increasing irradiation this charge cannot be fully collected due to trapping and incomplete depletion. As both effects can be reduced by increasing the sensor bias, the choice of the sensor concept must allow the application of elevated bias voltages without causing electrical breakdown. For the CMS pixel detector a maximum value of 500-600 V is foreseen. In addition to the radiation-induced effects there might be regions in the sensor with lower charge collection efficiency which have to be minimized by design optimization.

The irradiation induced effects in silicon are well known and can be divided into surface and bulk damage. The oxide charge increases until its saturation value of some 10^{12} cm^{-2} reached after some kGy. The concentration of interface traps also increases. Both effects influence the electric fields close to the surface and have to be considered when designing a sensor for radiative environments. The leakage current increases in proportion to the hadron fluence. When the hadron fluence exceeds about $5 \times 10^{13} \text{ n}_{\text{eq}}/\text{cm}^2$, the space charge in the depletion zone converts from positive (n -type) to negative (p -type) before increasing proportionally to the fluence. The change of the effective doping concentration shows a complex annealing behavior with exponential dependence on the sensor's temperature. In order to prevent reverse annealing, irradiated sensors must be kept cold.

The aim of this study is to compare two different design and technology options for the sensor part of the CMS pixel detector with respect to their signal collection properties.

¹All fluences are normalized to 1 MeV neutrons ($\text{n}_{\text{eq}}/\text{cm}^2$)

² $\eta = -\ln \tan(\Theta/2)$ where Θ is the track angle relative to the beam axis.

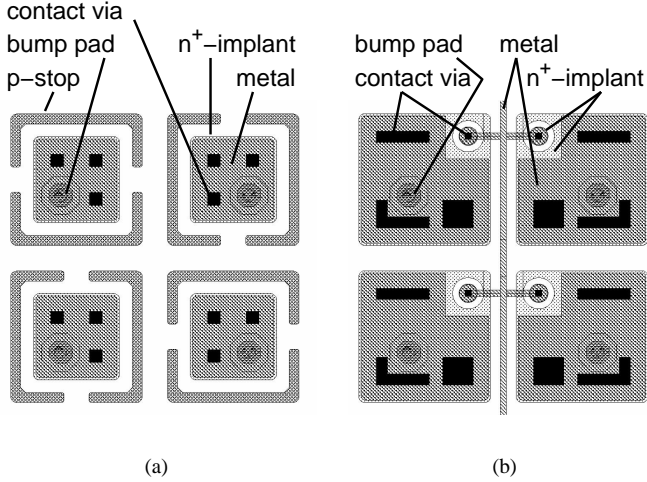


Fig. 1. Mask layout of the pixel sensors under study. Open p -stop rings (a) and p -spray with bias grid (b).

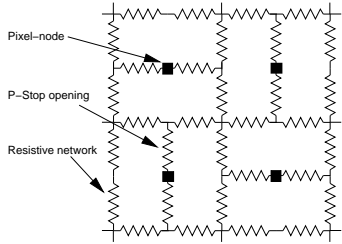


Fig. 2. Sketch of the “resistive network” formed by the electron accumulation layer and the p -stop openings. Each pixel node is connected to it by the openings in the p -stop rings.

II. SENSOR CONCEPTS UNDER STUDY

After the irradiation-induced space charge inversion of the substrate and the subsequent increase of the full depletion voltage, sensors might have to be operated partially depleted. Therefore an “ n -in- n ” concept has been chosen. In addition double-sided processing of these devices allows for the implementation of guard rings on the p -side of the sensor only, keeping all sensor edges at ground potential. The design of the guard rings has been optimized in the past [2]. The breakdown voltage exceeds by far the required value of about 600 V.

In order to readout the ohmic n -side of the sensor inter-pixel isolation has to be provided. Here p -stops are considered as well as the p -spray technique. The pixel-layout of the two design options investigated for this study are shown in fig. 1. In order to test the segmented devices on wafer with current-voltage (IV) measurements and to keep accidentally unconnected pixel cells close to ground potential, high resistive electrical connections between the pixels have been implemented. In the case of p -stops this was realized by openings in the p -stop implants. The fixed positive oxide charge builds up a electron accumulation that forms a “resistive network” to which all pixels are connected via the openings (see fig. 2). The properties of such “resistors” have been studied in detail in refs. [2] and [3]. According to previous investigations [3], [4] the most promising geometries feature small distances between

the n^+ -implants and quite large p -stop openings. Both are realized in the design under study shown in fig. 1a.

In addition we investigated prototypes featuring the moderated p -spray isolation technique. Here the isolating p -implant is performed without a photo-lithographic mask and therefore no structuring is possible. However punch-through biasing can be implemented. Its behavior is much less dependent on outer conditions like backside bias and radiation effects than the resistors formed by electron accumulation. The layout (see fig. 1b) is characterized by small gaps of $20\text{ }\mu\text{m}$ between the n^+ -implants and by a minimized biasing structure using small “bias dots” [5].

A batch of prototype pixel sensors containing devices with the pixel geometry described above was produced in 2001. Following the recommendation of the ROSE collaboration [6], oxygen enriched silicon was used to improve the post irradiation behavior.

In order to match the dimensions of the readout chip used for sensor studies miniature sensors containing 22×32 square pixels with a pitch of $125 \times 125\text{ }\mu\text{m}^2$ have been used. Although these dimensions differ slightly from the cell size used in CMS we are confident that the basic charge collection properties presented in this paper are not effected by the change of the cell size to $100 \times 150\text{ }\mu\text{m}^2$. Other properties, as for example the spatial resolution, have to be measured with the original configuration.

III. TEST PROCEDURE

Several miniature sensors of the two designs were bump bonded to readout chips of the type PSI30/AC30³ described in detail in ref. [7]. This chip allows one to force a sequential readout of all 704 pixel cells without zero suppression. All comparators are switched off by masking the pixels or setting the thresholds to very high values. The sampling time at the shaper is defined by an external hold signal. The shaping times of the preamplifier and the shaper were adjusted to prevent saturation of the preamplifier and shaper up to signals corresponding to about 1.5 minimal ionizing particles (m.i.p.). In the test beam setup a pin-diode was used to provide the external hold signal and to trigger the readout.

Some of the sensors were irradiated at the CERN PS in May 2003 after bump deposition but before being attached to the readout chips. The irradiation was performed at room temperature without bias. The fluences applied were 3, 8, and $11 \times 10^{14}\text{ n}_{\text{eq}}/\text{cm}^2$. In order to avoid reverse annealing the sensors were stored at -20°C after irradiation and warmed up to room temperature only for transport and bump bonding. For the irradiated sensors a special bump bonding procedure without heat application was used. The total time at room temperature was below 48 h and therefore all devices were still in the state of beneficial annealing at the measuring time. Prior to bump bonding all sensors were characterized with IV-measurements.

The bump bonded samples were tested at the CERN-SPS H2 beam line using 150 – 225 GeV pions. The pixel device

³PSI30 DMILL pixel readout chip was designed 1997 at Paul Scherrer Institut, Villigen, Switzerland, and translated 1998 to the Honeywell RCMOS IV process at 1. Physikalisches Institut of the RWTH Aachen, Germany.

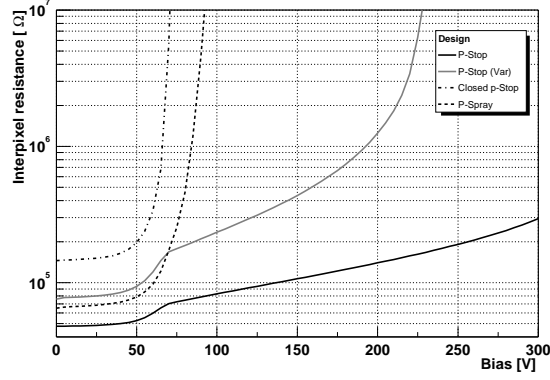


Fig. 3. Resistance between one pixel and all its neighbors as a function of the back side voltage. For comparison to the designs in fig. 1 (*p*-stop and *p*-spray) two other design options are also shown.

under test was situated in-between a four layer silicon strip telescope [8] with an intrinsic spatial resolution of about 1 μm . The whole set-up was placed in a 3 T magnet with the \vec{B} field parallel to the beam. The pixel detector was set either normal to the beam, or with a flat angle of 15° between the beam and the sensor surface. This paper only reports on data taken at normal incidence without magnetic field. The measurements performed in magnetic field and with a tilted are reported in ref. [9]. The irradiated sensors were operated at -20°C by the means using of water cooled Peltier elements.

IV. RESULTS

A. Inter-pixel resistance

While *p*-spray isolated devices naturally feature high inter-pixel isolation the inter-pixel resistance of the *p*-stop devices depends very much on the geometry of the openings in the *p*-stop rings and on the gap width.

Figure 3 shows the inter-pixel resistance of different pixel designs as a function of the sensor bias. An array of 5×5 pixels was grounded while the potential of the center pixel was set to +1 V. The current flowing into this pixel was measured in dependence of the back side voltage. In order to illustrate the effect of the *p*-stop openings in the *p*-stop design (fig. 1a), an identical design with closed *p*-stops, a different *p*-stop geometry, and the *p*-spray design (fig. 1b) are also shown.

As the depletion starts from the back side (“*n*-in-*n*”), part of the current flows through the bulk before full depletion is reached and the corresponding inter-pixel resistance is low. With progressing depletion this channel is pinched off and the resistance in the fully isolated devices increases rapidly by several orders of magnitude. In the devices featuring *p*-stop openings a residual current flows over the electron accumulation layer. However, with the backside bias being increased further this electron channel also starts to be pinched off. This is visible in fig. 3 for the curve labeled “*p*-stop (Var)” at bias above 200 V.

The design called “*p*-stop” shows no pinch off up to 300 V. Its inter-pixel resistance at backside voltage of 150 V is only about 100 k Ω . This results in wide signal spreading along the resistive channels. The test beam data with the unirradiated

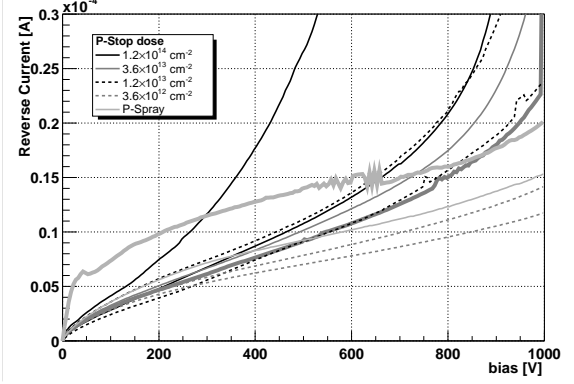


Fig. 4. IV curves of each two sensors (open *p*-stops, fig. 1a, with different *p*-stop implantation doses irradiated to $\Phi = 8 \times 10^{14} \text{ n}_{\text{eq}}/\text{cm}^2$, measured at -20°C . For comparison two *p*-spray sensors (fig. 1b) are also plotted. The devices used in the test beam are represented by the bold lines.

device was therefore taken at 300 V bias voltage where the inter-pixel resistance reaches a value of 300 k Ω . At this bias voltage we observe a reduced spread of the collected charge over several pixels.

For irradiated sensors the resistance of the electron accumulation layer is much higher (in the order of G Ω), more or less independent on the designs [2], [3].

B. Characteristics and Noise

The current vs. voltage characteristic is a very sensitive tool used in detecting possible problems in a sensor. Especially after irradiation an early current increase is an indication for electrical breakdown. Early breakdown accompanied by noise increase was previously observed in irradiated *p*-stop isolated devices [3], [10] and is considered to be their major drawback.

To improve the breakdown behavior of the *p*-stop devices, the implantation dose of the *p*-stop implant has systematically been reduced from the typically used 10^{14} cm^{-2} down to the *p*-spray level of $3 \times 10^{12} \text{ cm}^{-2}$. The IV-characteristics of these devices after a proton irradiation of $\Phi = 8 \times 10^{14} \text{ n}_{\text{eq}}/\text{cm}^2$ are plotted in fig. 4 together with two *p*-spray devices. It is seen that the current and the slope of the curve decreases with decreasing *p*-stop dose. The sensors with a *p*-stop dose of $3 \times 10^{12} \text{ cm}^{-2}$ show an IV-characteristic similar to the one of the *p*-spray sensors.

In total six sensors of the two designs have been bump bonded to readout chips. Since a full non zero-suppressed readout is possible, the noise of each pixel can be easily determined. In fig. 5 the bias dependence of the average pixel noise is shown for two sensors of each type unirradiated and irradiated to $8 \times 10^{14} \text{ n}_{\text{eq}}/\text{cm}^2$. 12 ADC-counts correspond to a noise of about 400 electrons. However this number represents only an approximate estimation as an exact calibration was not yet performed.

For the irradiated sensors no distinct bias dependence of the noise is observed. The noise of the irradiated *p*-spray sensors is about 1 ADC count higher than the noise of the *p*-stop sensors. An additional *p*-spray sensor irradiated to $1.1 \times 10^{15} \text{ n}_{\text{eq}}/\text{cm}^2$

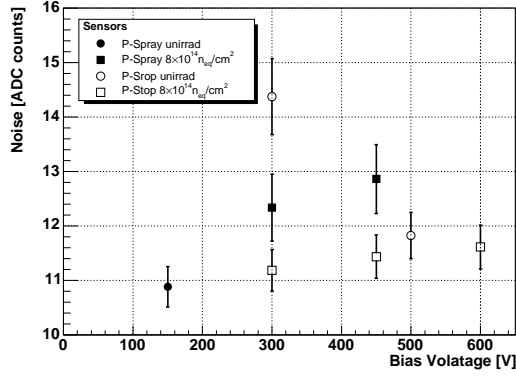


Fig. 5. Bias dependence of the noise on four bump bonded pixel sensors. The central value indicates the mean and the error bar the sigma of a Gaussian fit to the noise distribution of all connected pixels in each sensor.

(not plotted in fig. 5) shows a noise of 17.4 ADC counts at 600 V, which is still tolerable.

The noise of the unirradiated *p*-stop sensor at 300 V is quite high (14.4 ADC counts) and decreases with increasing bias to 11.8 ADC counts at 500 V. This is because the inter-pixel resistance increases and the coupling between pixels becomes weaker.

The error bars in fig. 5 represent the sigma of a Gaussian fit to noise distribution in each sensor and therefore the variation of the noise with the sensor. We observe no localized regions of high noise.

From the absence of noisy regions and from the shape of the IV-curves we conclude that electrical breakdown in *p*-stop isolated silicon detectors can be avoided by reducing the implantation dose to about 10^{13} cm^{-2} .

C. Charge Collection Properties

The high energy pion beam of the CERN SPS (150-225 GeV) together with a high precision beam telescope [8] allows for detailed study of the pixel sensor on a $1 \mu\text{m}$ -level. Of particular interest is the study of the charge collection efficiency as a function of the particle impact point in order to locate “blind” spots within the pixel cell.

Figure 6 shows the mean total cluster charge deposited by perpendicular tracks as function of the pion impact position. The area shown represents one square pixel cell with a pitch of $125 \mu\text{m}$. The cluster signal was obtained by summing the signals of the 3×3 pixels around the impact point (pixel threshold: 20 ADC counts, cluster threshold: 50 ADC counts). The average amplitude of the cluster signals are listed in table I. In addition values are given for the signal amplitude in the pixel center and regions with reduced charge collection.

The cluster size was determined by counting the number of pixels above threshold in the direct neighborhood of the impact point. Its average value as a function of the applied pixel threshold is plotted in fig. 7. The average cluster size for a threshold of 60 ADC counts is listed in table I.

To calculate the signal over noise ratio, only the signal in the “hit pixel”, the pixel pointed to by the beam telescope, is taken into account. It is obtained by histogramming the

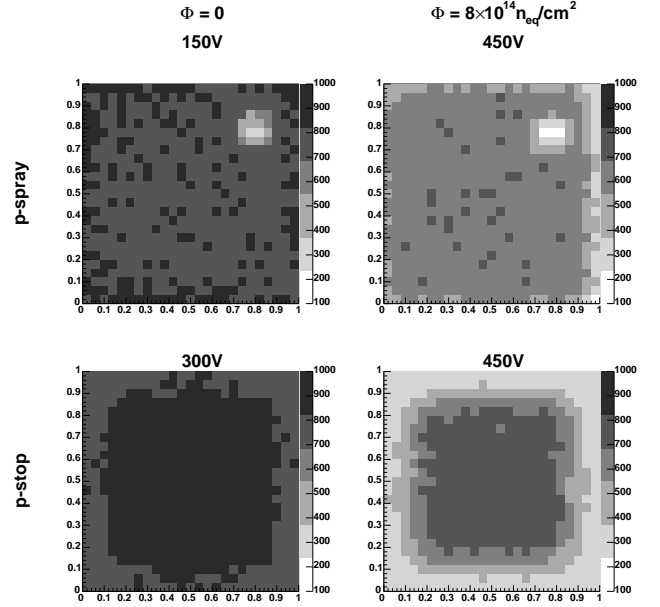


Fig. 6. Cluster charge as function of the pion point of incidence. The area shown represents one pixel cell of $125 \times 125 \mu\text{m}^2$, the charge is given in ADC counts. The *p*-spray (above) and the *p*-stop (below) designs are shown for different bias voltages.

charge in this pixel and calculating its mean value, which is also listed in table I. Values are also given for tracks passing the the pixel center. The signal to noise ratio was calculated by dividing the average signal in the hit pixel by its noise. A more detailed discussion of the signal to noise ratio including its bias dependence is given in ref. [9].

1) *Unirradiated p-spray sensors:* For unirradiated *p*-spray sensors a very homogeneous average cluster signal of about 800 ADC counts is observed. At the position of the bias dot it drops to less than half of this value. As this critical area represents only 2–3 % of the total surface the average collected signal is only weakly affected.

On average about 89 % of the charge is collected by the hit pixel. For tracks in the pixel center this number increases to 96 %. Consequently, the average cluster size is below 1.3 pixels. The large fraction of the cluster signal being collected by one pixel leads to a high signal over noise ratio of 65.

2) *Irradiated p-spray sensors:* After irradiation with a fluence of $\Phi = 8 \times 10^{14} \text{ n}_{\text{eq}}/\text{cm}^2$ the value of the total collected cluster charge is reduced by about 25 %. Furthermore an additional area of reduced charge collection appears at the metal line connecting the bias dots. The collected cluster charge of particles hitting this region is almost 40 % smaller than those hitting the pixel center. As there is no direct contact between this metal line and the silicon below, this behavior (also reported in ref. [11]) was a priori unexpected and not yet fully understood. It seems plausible that the charge loss is caused by capacitive coupling. Before irradiation the metal line is shielded by the conductive *p*-spray layer. However after irradiation the *p*-spray layer behaves like a (bad) insulator and a charge drifting below this layer can induce an electrical

TABLE I
SUMMARY OF TEST BEAM RESULTS.

Φ [n _{eq} /cm ²]	Bias [V]	Mean Cluster Signal [ADC]			Signal in hit pixel [ADC]		Cluster Size at 60 ADC	Noise [ADC]	S/N	Efficiency at 60 ADC
		Average	Center	Border	Average	Center				
<i>p-spray</i>										
0	150	800	803	dot: 366	710	768	1.26	10.9	65	99.69 %
8×10^{14}	450	599	647	dot: < 253 line: 342	533	612	1.22	12.9	41	98.56 %
1.1×10^{15}	600	533	567	dot: < 290 line: 314	457	521	1.21	17.4	26	99.23 %
<i>p-stop</i>										
0	300	847	905	765	424	569	3.36	14.4	29	99.67 %
3×10^{14}	300	535	702	361	431	665	1.43	11.5	37	99.67 %
8×10^{14}	450	539	718	323	465	700	1.35	11.4	41	99.32 %

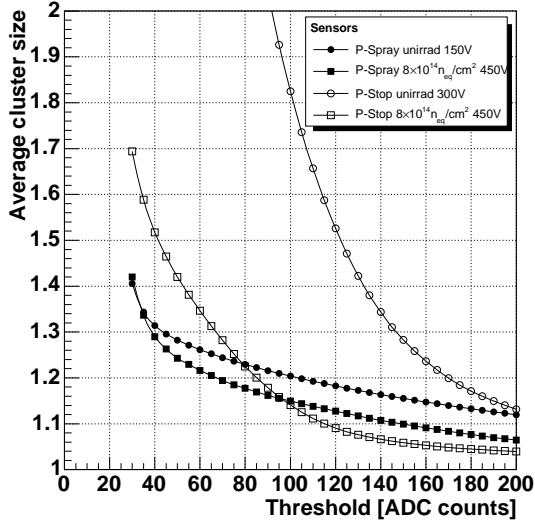


Fig. 7. Average cluster size for the different sensors as function of the pixel threshold.

signal on the bias line above. Since the total affected area is under 10 %, the signal averaged over the whole pixel cell is about 7 % smaller than the signal collected in the central pixel region.

The charge sharing between pixels is not effected by the irradiation. Still 89 % of the cluster charge is collected by one pixel and the average cluster size decreases only a little. As the signal height decreases and the noise slightly increases, the signal over noise ratio of this irradiated sensor decreases to 41.

For the *p-spray* sensor irradiated to $\Phi = 11 \times 10^{14}$ n_{eq}/cm², the general behavior remains unchanged. However, due to the reduced cluster signal and the increased noise, the signal over noise ratio is further reduced. A more detailed discussion of the charge collection dependence on the particle fluence and the bias voltage is presented in ref. [9].

3) *Unirradiated p-stop sensors*: The highest average cluster signals were observed in the center of an unirradiated *p-stop* sensor, 905 ADC counts, which is about 12 % larger than the maximum in the *p-spray* devices. However, one has to take into account the use of 300 V bias voltage in order to reduce the charge spread due to the resistive connections between

pixels. Even at such a high bias voltage the average cluster size, using a pixel threshold of 60 ADC counts, is above 3, much higher than in the other investigated sensors. Even if a pixel is hit centrally it carries only 63 % of the total cluster signal (in average it is only 50 %). Close to the pixel border the cluster signal decreases by about 15 % compared to the central region. As the hit pixel carries only a small fraction of the total cluster signal, the signal to noise ratio is only 29.

4) *Irradiated p-stop sensors*: Due to the irradiation induced increase of the inter-pixel resistance the average cluster size of the irradiated *p-stop* sensors decreases to values below 1.5. At the same time the fraction of the cluster signal collected by the hit pixel increases to 85 %, the same level as in the *p-spray* sensors. While the average cluster charge in the sensor irradiated to $\Phi = 8 \times 10^{14}$ n_{eq}/cm² decreases by about 20 % compared to the unirradiated sensor, the charge collected by the hit pixel stays about unchanged. When the pixel is hit in its center, the charged collected by the hit pixel even increases. The concentration of signal charge on one pixel leads to an increase of the signal over noise ratio to 41, exactly the same value as the *p-spray* sensor irradiated to the same fluence.

The cluster charge for tracks close to the pixel border decreases to half of the value for tracks in the center. The reason for this significant charge loss is not fully understood but the following explanation seems possible: The electron accumulation layer between the *p-stops* adjusts to the same potential as the pixel implants due to the openings in the *p-stops*. For this reason the layer also collects signal charge. For the unirradiated sensor the surface mobility in the electron accumulation layer is high enough to allow a quick transfer of the collected charge to the next readout *n*⁺-implant. Therefore the average cluster size in the unirradiated sensor is very high. After irradiation the mobility of free charge carriers close to the surface is strongly reduced and the number of surface traps increases. The charge drift to the next readout *n*⁺-implant is slower and a significant fraction of the signal collected in the accumulation layer might not reach it in time. Hence the cluster size in the irradiated *p-stop* sensor is much smaller.

D. Particle Detection Efficiency

In the final operation of the pixel detector the important figure of merit is the probability for actually detecting a particle penetrating the detector. In order to translate the charge

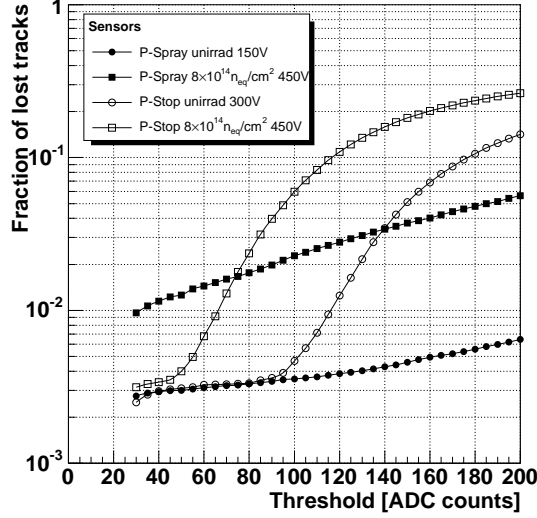


Fig. 8. Fraction of undetected tracks in the pixel detector as function of the applied threshold.

collection behavior discussed in the previous sections into efficiency measures, realistic thresholds have been required. If the pixel pointed to by the beam telescope or a direct neighbor was above the threshold, the track was counted as detected. A cluster threshold was not applied. Regions of defect bump bonding or noisy pixels were excluded from this analysis.

The choice of the threshold values is somewhat arbitrary as the amplitude of the signal output was not yet properly calibrated. As the noise of all sensors is between 11 and 13 ADC counts, a threshold of 60 ADC counts, about five times the noise, was chosen to estimate the efficiency numbers. This value corresponds roughly to a signal charge between 2000 and 2200 electrons. The probability for detecting a particle with a pixel threshold of 60 ADC channels is given in table I. In all cases it is above 98 %.

1) *p-spray sensors*: The inefficiency as a function of the threshold is plotted in fig. 8 for both designs under study, and for proton fluences of 0 and $8 \times 10^{14} \text{ n}_{\text{eq}}/\text{cm}^2$. Here a difference between the designs is visible. In the unirradiated *p-spray* design the charge loss due to the bias dot is small enough not to cause an inefficiency if the pixel threshold is below 100 ADC counts. For higher thresholds the lost tracks start to concentrate around this area. In the case of the irradiated *p-spray* sensor the probability for losing a track hitting the bias dot is higher due to the lower total charge. Already at low threshold the total inefficiency is about 1 %. With increasing threshold the inefficiency rises as well. Tracks hitting the region below the metal line of the bias grid start to contribute, starting from the corner of the pixel and growing along the pixel edge below the metalization. When the threshold exceeds 130 ADC channels, a small accumulation of lost tracks can be found also in the corners opposite to the metal line. As the total problematic area is quite small, the slope of the increase is limited and the inefficiency does not exceed 4 % even at high threshold (e.g. 160 ADC counts).

2) *p-stop sensors*: For the *p-stop* designs the situation looks different. As the charge loss in the pixel edge region is less drastic, the efficiency at low threshold is also above 99.5 % also for the irradiated sensor. However, as the less efficient region at the pixel edge covers a significant fraction of the area, the inefficiency increases rapidly with increasing threshold. The lost tracks accumulate at the pixel corners. With increasing threshold the regions of lower efficiency grow along the pixel edges.

Although the irradiated *p-stop* sensor reach a better efficiency at a threshold of 60 ADC counts, it has to be stressed that the high slope of the inefficiency displays a potential risk. A small threshold variation can lead to a non-tolerable inefficiency above 5 %. The *p-stop* sensor irradiated to $8 \times 10^{14} \text{ n}_{\text{eq}}/\text{cm}^2$ has also been measured at a bias voltage of 600 V. The higher bias increases the collected charge and the detection efficiency, although not significantly.

The situation in the test beam with perpendicular tracks without magnetic field is well suited for characterizing the charge collection properties of the sensors with high precision. In the final experiment, however, the signal charge will always be spread over a certain area due to the track inclination and the Lorentz drift. Therefore the effect of small regions with reduced charge collection will be suppressed.

V. CONCLUSIONS

Silicon pixel sensors of “*n-in-n*” type featuring *p-spray* and *p-stop* isolation have been irradiated to proton fluences up to $1.1 \times 10^{15} \text{ n}_{\text{eq}}/\text{cm}^2$. All sensors show IV-curves with a breakdown voltage well above 600 V without localized noisy regions. In the case of *p-stop* sensors this was achieved by reducing the *p-stop* implantation dose to about 10^{13} cm^{-2} .

The charge collection studies were performed with bump bonded samples in a high energy pion beam. The total charge collected after the highest fluence applied was about 60 % of the value obtained with unirradiated sensors independent of the sensor design. The main results for the different sensor type are the following.

p-spray sensors

- The *p-spray* devices showed a very homogeneous charge collection also in the inter-pixel regions.
- The bias dots represent an area with strongly reduced charge collection, leading to a loss of particle detection efficiency of about 1 % after an irradiation fluence of $8 \times 10^{14} \text{ n}_{\text{eq}}/\text{cm}^2$.
- For irradiated sensors the metal line of the bias grid additionally reduces the charge collection.
- The particle detection efficiency after this fluence still exceeds 98 % and is only moderately dependent on the pixel threshold.

p-stop sensors

- In the unirradiated sensor the signal is spread over many pixels.
- After irradiation this spread is strongly reduced.
- The most inefficient region is located in between the pixels. The cluster signal of a track hitting an irradiated

sensor close to the pixel border is only half of the size of a central hit.

- The particle detection efficiency is above 99 % at low threshold but drops drastically for thresholds higher than about 110 ADC counts for the unirradiated sensor and 65 ADC counts for the sensor irradiated to $8 \times 10^{14} \text{ n}_{\text{eq}}/\text{cm}^2$.

The steep increase of lost tracks seems to be the major drawback of the p -stop sensors and has to be further investigated. A possible improvement of the charge collection in the inter-pixel region might be possible, if the pattern of the resistive inter-pixel connections is changed. Every pixel should not be coupled resistively to an overall network as indicated in fig. 2, but only to its direct neighbors. In this case also the large spread of the signal charge in the unirradiated sensor will be reduced. Such devices were already built and will be investigated in the near future.

ACKNOWLEDGMENT

The authors would like to thank Silvan Streuli from ETH Zürich and Fredy Glaus from PSI for their enormous effort in bump bonding, Kurt Böisinger from the workshop of the University of Zürich for the mechanical construction, Maurice Glaser and Michael Moll from CERN for carrying out the irradiation, and György Bencze and Pascal Petiot from CERN for the H2-beam line support. Thanks are also due to Danek Kotlinski for the very useful discussions and for sharing his detailed knowledge of the pixel control and readout system. Last but not least we gratefully acknowledge Roland Horisberger from PSI for explaining all details of the readout chip. Without his advice this work would not have been possible.

REFERENCES

- [1] "CMS tracker," CERN, Geneva, Switzerland, Technical Design Report LHC 98-6, 1998.
- [2] K. Kaufmann, "Development of radiation hard pixel sensors for the CMS experiment," Ph.D. dissertation, Universität Zürich, Zürich, Switzerland, 2001.
- [3] G. Bolla *et al.*, "Sensor developement for the CMS pixel detector," *Nucl. Instr. and Meth.*, vol. A 485, pp. 89–99, 2002.
- [4] —, "Irradiation studies of silicon pixel detectors for CMS," *Nucl. Instr. and Meth.*, vol. A 501, pp. 160–163, 2003.
- [5] T. Rohe *et al.*, "Design and test of pixel sensors for the ATLAS pixel detector," *Nucl. Instr. and Meth.*, vol. A 460, pp. 55–66, 2001.
- [6] G. Lindström *et al.*, "Radiation hard silicon detectors – developments by the RD48 (ROSE) collaboration," *Nucl. Instr. and Meth.*, vol. A 466, pp. 308–326, 2001.
- [7] D. Meer, "Bau und Messen eines Multichip Pixelmodules als Prototyp für den CMS-Tracker," Diplomarbeit, Eidgenössische Technische Hochschule, Zürich, Switzerland, Mar. 2000.
- [8] C. Amsler *et al.*, "A high resolution beam telescope," *Nucl. Instr. and Meth.*, vol. A 480, pp. 501–507, 2002.
- [9] A. Dorokhov *et al.*, "Test beam measurements on the silicon sensors of the CMS pixel detector," presented at the 6th International Conference on Large Scale Applications and Radiation Hardness of Semiconductor Detectors, Sept. 2003, submitted for publication in *Nucl. Instr. and Meth. A*. [Online]. Available: <http://arxiv.org/abs/physics/0311050>
- [10] D. Robinson *et al.*, "Noise studies of n-strip on n-bulk silicon microstrip detectors using fast binary readout electronics after irradiation to $3 \times 10^{14} \text{ p cm}^{-2}$," *Nucl. Instr. and Meth.*, vol. A 426, pp. 28–33, 1999.
- [11] T. Lari *et al.*, "Test beam results of ATLAS pixel sensors," presented at the Proceedings of the International Workshop on Semiconductor Pixel Detectors for Particles and X-Rays (PIXEL2002), 2002. [Online]. Available: <http://www.slac.stanford.edu/econf/C020909/>